

**Folate-Containing Reduction-Sensitive Lipid-Polymer Hybrid Nanoparticles for Targeted Delivery of Doxorubicin**

| | |
|-------------------------------|---|
| Journal: | <i>Biomaterials Science</i> |
| Manuscript ID: | BM-ART-12-2014-000462.R1 |
| Article Type: | Paper |
| Date Submitted by the Author: | 07-Feb-2015 |
| Complete List of Authors: | Wu, Bo; Wuhan University, Yu, Ping; Wuhan University, Department of Chemistry Cui, Can; Wuhan University, Wu, Ming; Wuhan University, Zhang, Yang; Wuhan University, Department of Chemistry Liu, Lei; Wuhan University, ; Wuhan University, Department of Chemistry Wang, Cai-Xia; Wuhan University, Department of Chemistry Zhuo, Renxi; Wuhan University, China, Dept of Chemistry Huang, Shi-Wen; Wuhan University, Department of Chemistry |
| | |

1 The table of contents

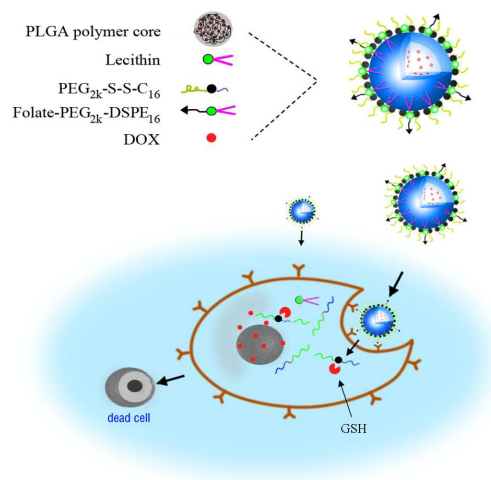
2 Title: Folate-Containing Reduction-Sensitive Lipid-Polymer Hybrid Nanoparticles for

3 Targeted Delivery of Doxorubicin

4 Highlight: Lipid-polymer hybrid nanoparticles (FLPNPs) containing folate targeted

5 ligand and reduction-sensitive outer layer was developed to enhance drug

6 delivery efficacy in vitro and in vivo



7

Page 1 of 30

1 **Folate-Containing Reduction-Sensitive Lipid-Polymer Hybrid**
2 **Nanoparticles for Targeted Delivery of Doxorubicin**

3
4 Bo Wu^a, Ping Yu^a, Can Cui^a, Ming Wu^a, Yang Zhang^a, Lei Liu^a, Cai-Xia Wang^a,
5 Ren-Xi Zhuo^a and Shi-Wen Huang^{a*}

6 ^a Key Laboratory of Biomedical Polymers, Ministry of Education, Department of
7 Chemistry, Wuhan University, Wuhan 430072, PR China

8
9 **ABSTRACT:** The development and evaluation of folate-targeted and
10 reduction-triggered biodegradable nanoparticles are introduced for the research of
11 targeted delivery of doxorubicin (DOX). This type of Folate-targeted lipid-polymer
12 hybrid nanoparticles (FLPNPs) are comprised of a poly-(D, L-lactide-co-glycolide)
13 (PLGA) core, a soybean lecithin monolayer, a monomethoxy-poly-(ethylene
14 glycol)-S-S-hexadecyl (mPEG-S-S-C₁₆) reduction-sensitive shell, and a folic
15 acid-targeted ligand. FLPNPs exhibited high size stability but fast disassembly in
16 simulated cancer cells reductive environment. The experiments on release process in
17 vitro revealed that as a reduction-sensitive drug delivery system, namely, FLPNPs
18 released DOX faster in the presence of 10 mM dithiothreitol (DTT). Results in flow
19 cytometry, confocal image and in vitro cytotoxicity assay revealed that FLPNPs
20 further enhanced cell uptake and generated higher cytotoxicity against human
21 epidermoid carcinoma in the oral cavity than non-targeted redox-sensitive and
22 targeted redox-insensitive controls. Furthermore, in vivo animal experiments

Page 2 of 30

1 demonstrated that systemic administration of DOX-loaded FLPNPs remarkably
2 reduced the tumor growth. Experiments on biodistribution of DOX-loaded FLPNPs
3 showed that an increasing amount of DOX accumulated in the tumor. Therefore,
4 FLPNP formulations are proved to be a stable, controllable and targeted anticancer
5 drug delivery system.

6 **KEYWORDS:** drug delivery, folate-targeted, reduction-sensitive, lipid-polymer
7 hybrid, nanoparticles

8

9 **1 INTRODUCTION**

10 Over the past two decades, more than two dozen nanosized therapeutics have been
11 approved for clinical use, and a large number of other nanosized products are in
12 clinical trials.¹ In all kinds of nanosized therapeutics, liposomes and biodegradable
13 polymeric nanoparticles (NPs) are the most representative classes of drug
14 nanocarriers.^{2, 3} In view of various advantages of polymeric nanoparticles and
15 liposomes, a new type of drug delivery system named lipid-polymer hybrid
16 nanoparticles (LPNPs) which combined the positive attributes of both liposomes and
17 polymeric NPs into a single delivery system has been developed.^{4, 5} The LPNPs
18 consists of three parts: a biodegradable hydrophobic polymeric core to encapsulate
19 hydrophobic drugs; a monolayer of phospholipids surrounding the core to increase
20 system biological compatibility; and a hydrophilic polymeric layer outside the lipid to
21 keep formulation stability and enhance systemic circulation lifetime.⁶ In comparison
22 to conventional nanoparticle formulations, the LPNPs have been demonstrated to

Page 3 of 30

1 exhibit unique strengths of polymeric nanoparticles and liposomes, while excluding
2 some intrinsic limitations.⁷

3 To further improve the therapeutic efficiency and reduce side effects, a better
4 strategy is to develop molecular targeted nanoparticle therapeutic carriers. Various
5 targeted moieties or ligands have been employed to improve the cellular uptake within
6 target cells via receptor-mediated endocytosis. Among them, folate is widely used,
7 since it can also avoid the attacks of drugs on normal tissues. Folate can bind very
8 firmly to folate receptors (FRs, $K_d \sim 10^{-10}$ M).⁸ Several human tumors such as ovarian
9 cancer, breast cancer and epidermoid carcinoma of the oral cavity overexpress FRs.⁹
10 ¹⁰ Here, we further improve the formulation of LPNPs by introducing targeted ligands
11 to enhance the effectiveness of cancer chemotherapy. One way of realizing such a
12 design is to conjugate targeted ligands onto the surface of LPNPs. A folate group
13 covalently attached to hydrophilic polymer was used to form the shell of LPNPs. As
14 expected, these modified LPNPs will selectively and targetedly suppress KB cells
15 growth, with reduced cardiac toxicity of doxorubicin (DOX).

16 In addition, stimuli-insensitivity is still a major limitation on LPNPs drug delivery
17 in intracellular drug release. Stimuli-sensitive drug delivery systems which can release
18 anticancer drugs in response to an intrinsic biosignal are widely studied and used in
19 cancer therapy.¹¹⁻¹⁴ This strategy has been proved to improve the therapeutic efficacy
20 and reduce severe side effects of anticancer drugs.¹⁵⁻¹⁸ For example, redox-sensitive
21 drug delivery systems have been designed and explored for enhancing cancer therapy
22 based on the huge different concentrations of cytoplasmic glutathione (GSH) between

Page 4 of 30

1 cytosol (2-10 mM) and extracellular fluids (2-20 μ M).¹⁹⁻²² Disulfide linkages, which
2 are stable under normal physiological conditions, may be prone to rapid cleavage in
3 response to reductive environment of intracellular fluids in cancer cells through
4 thiol-disulfide exchange reactions.^{23, 24} As the result of a sudden intracellular burst of
5 encapsulated drugs caused by the cleavage of disulfide bonds in cancer cells,
6 redox-sensitive drug nanocarriers can achieve high drug uptake efficiency and good
7 efficacy.²⁵ Our earlier work on the preparation of reduction-sensitive micelles also
8 demonstrated the advantages of the amphiphilic reduction-sensitive polymer of
9 monomethoxy-poly-(ethylene glycol)-S-S-hexadecyl (mPEG-S-S-C₁₆) for the
10 effective intracellular delivery of anticancer drugs.²⁶

11 Thus, it is ideal if a new type of NPs could retain the advantages of traditional
12 hybrid nanoparticles, and it also has redox-sensitivity and active targeting ability at
13 the same time. In this study, we designed a new type of hybrid nanoparticles FLPNPs
14 using folate as targeted ligand and an amphiphilic reduction-sensitive polymer to
15 achieve intracellular release, and then improve therapeutic effect. The FLPNPs
16 comprised of a biodegradable hydrophobic poly-(D, L-lactide-co-glycolide) (PLGA)
17 core, a soybean lecithin monolayer, an outer corona layer of an amphiphilic
18 redox-sensitive polymer, and a folic acid-targeted ligand (Fig. 1A). The amphiphilic
19 polymer mPEG-S-S-C₁₆ containing disulfide bond was employed as a
20 reduction-sensitive shell, which can keep the stability of this formulation and server as
21 a switch to trigger drug release. This targeted and redox-sensitivity FLPNPs will
22 combine the desirable characteristics of both traditional hybrid nanoparticles and

Page 5 of 30

1 redox-responsive micelles, and thus will evolve a fascinating opportunity for
2 development of new drug delivery systems.

3

4 **2 EXPERIMENTAL SECTION**

5 **2.1 Materials and methods**

6 All chemicals were obtained from Sigmae Aldrich (St. Louis, MO) unless
7 otherwise noted. 1,2-distearoyl-sn-glycero-3-phosphoethanolamine-N-car-
8 boxy(polyethylene glycol) 2000 (DSPE-PEG_{2k}), and
9 1,2-distearoyl-sn-glycero-3-phosphoethanolamine-N-car-boxy(polyethylene glycol)
10 2000-Folate (DSPE-PEG_{2k}- FOL) were provided by Avanti Polar Lipids Inc. (Avanti,
11 USA). Poly [D, L-lactide-co-glycolide] (PLGA, 75:25, MW: 90,000–126,000) and
12 Lecithin were purchased from Sigma-Aldrich (St. Louise, MO, USA). N, N-dimethyl
13 formamide (DMF), DL-Dithiothreitol (DTT), triethylamine (TEA) and
14 dimethylsulfoxide (DMSO) were all purchased from Shanghai Chemical Co.. All
15 solvents used in this study were HPLC grade. Polymer monomethoxy-poly (ethylene
16 glycol)-S-S-hexadecyl (mPEG_{2k}-S-S-C₁₆) was synthesized using a method reported in
17 our previous work.²⁶ Briefly, C₁₆-S-S-COOH (0.52 g, 1.2 mM), DCC (0.272 g, 1.32
18 mM), and DMAP (0.03 g, 0.26 mM) were added to an mPEG solution (0.4 g, 0.2 mM)
19 in 20 mL of anhydrous dichloromethane. After stirring at 28 °C overnight, the mixture
20 was filtered and the solvent was evaporated under reduced pressure. The crude
21 product was washed three times with ethyl ether to obtain a white solid (yield 83%).
22 The synthesis of mPEG-C-C-C₁₆ polymer was similar to that of mPEG-S-S-C₁₆

Page 6 of 30

1 polymer (yield 85%).

2 Human oral cavity squamous cell carcinoma cells (KB cell) and the african green
3 monkey SV40-transformed kidney fibroblast cells (COS-7) were purchased from the
4 China Center for Type Culture Collection (Wuhan University) and cultured in RPMI
5 1640 medium or folate-free RPMI 1640 medium, supplemented with 4×10^{-3} M
6 L-glutamine, 10% fetal bovine serum (FBS) and 1% antibiotics (100 U mL^{-1} penicillin
7 and 100 m g mL^{-1} strepto-mycin) at $37 \text{ }^\circ\text{C}$ in a humidified atmosphere containing 5%
8 CO_2 .

9 Female athymic BALB/c-nu nude mice (4–6 weeks old, 18 ± 2 g) were purchased
10 from Wuhan University experimental animal center/Animal Biosafety Level 3
11 Laboratory (ABSL-3 lab) (Wuhan, China). All animals received care in compliance
12 with the guidelines outlined in the Guide for the Care and Use of Laboratory Animals
13 and the procedures were approved by the Wuhan University of China Animal Care
14 and Use Committee.

15 **2.2. Preparation of of FLPNPs**

16 The FLPNPs were prepared using a previously reported Single-Step Assembly
17 method.^{27,28} In brief, prior to the FLPNPs preparation, the doxorubicin hydrochlorate
18 (DOX·HCl) was stirred with twice the molar amount of TEA in DMF for 10 h to
19 obtain lipophilic DOX base. 5mg DOX was dissolved in 10mL of DMF. Then the
20 polymer of PLGA (40mg) was added to the solution and stirred at room temperature
21 for 2h. DSPE-PEG_{2k}-Folate, mPEG-S-S-C₁₆ and lipid lecithin (weight ratio 1/9/3,
22 total lipids 12 mg) were dissolved in 30mL of 4wt % ethanol aqueous solution at 65°C ,

Page 7 of 30

1 and the DOX/PLGA solution was added dropwise under gentle stirring. Then, the
2 mixed solution was vortexed vigorously for 3 mins followed by dialyzing against
3 ultrapure water at 25 °C for 48h. Afterwards, the solution was filtered through a
4 syringe filter (pore size = 0.45µm) to remove the unloaded DOX. Finally, the
5 nanoparticles were concentrated using Amicon Ultra-4 centrifugal filter (Millipore,
6 Molecular-weight cut-off: MWCO = 8 000). To serve as a control, LPNPs were also
7 prepared by the above process, and DSPE-PEG_{2k}-FOL was replaced by DSPE-PEG_{2k}.
8 To serve as a control, a reduction-insensitive polymer mPEG-C-C-C₁₆ with an
9 analogous structure but without a disulfide bond was also prepared. Targeted
10 redox-insensitive control (redox-insensitive FLPNPs) was similarly prepared as a
11 control, and mPEG-C-C-C₁₆ was replaced by mPEG-S-S-C₁₆. DOX-free nanoparticles
12 were also prepared using above protocol but without DOX.

13 **2.3. Characterizations and reduction-triggered disassembly of FLPNPs**

14 The particle size and size distribution of the drug loaded nanoparticles were
15 measured by dynamic light scattering (DLS, 90Plus, Brookhaven Instruments Co.
16 USA). Transmission electron microscopy (TEM, JEM-100CX II) was used to
17 observe the micelle morphology.

18 The disassembly of FLPNPs in response to 20 µM and 10 mM reductive DTT in
19 PBS (0.1 M, pH 7.4) was monitored by DLS, using redox-insensitive FLPNPs as a
20 control. Briefly, to glass cells containing 2.5 mL solution of FLPNPs, DTT was added
21 to obtain the required concentration. The solution was placed at 37 °C and monitored
22 using DLS after 4 h incubation.

Page 8 of 30

1 **2.4. Drug encapsulation efficiency (EE) and loading efficiency (LE)**

2 To evaluate the drug encapsulation efficiency (EE) and loading efficiency (LE), a
3 predetermined aliquot of DOX-loaded nanoparticles was collected by freeze-drying,
4 and then the dry nanoparticles were dissolved in DMSO. After that, the DOX
5 concentration in DMSO was measured by fluorescence measurement using a
6 calibration curve constructed from DOX solutions with different DOX concentrations.
7 The EE is calculated as (actual amount of drug encapsulated in nanoparticles) / (initial
8 amount of drug used in the fabrication of nanoparticles) $\times 100\%$. $LE(\%) = (\text{amount of}$
9 $\text{the drug in particles} / \text{amount of the feeding material and drug}) \times 100\%$.

10 **2.5. Controlled drug release**

11 0.5 mL of the DOX-loaded FLPNPs was transferred into a dialysis tube (MWCO
12 8000). Then, it was immersed into a tube containing 10 mL of PBS (10 mM , pH 7.4)
13 with or without 10 mM DTT in a shaker shaken at 120 rpm and 37 °C. At designated
14 intervals, 5 mL of the external buffer was replaced with the corresponding fresh buffer
15 solution. DOX quantity was determined by fluorescence measurement (excitation at
16 485 nm). The error bars were obtained from triplicate samples.

17 **2.6. In vitro cellular uptake**

18 Confocal laser scanning microscope (CLSM, Nikon, TE2000, EZ-C1, Japan) was
19 used to examine the intracellular distribution of DOX. KB cells were seeded on slides
20 at a density of 5.0×10^4 cells/well in 1 mL of folic acid deficient 1640 medium
21 containing 10% FBS. The cells were then incubated with FLPNPs, LPNPs or Free
22 DOX at a final DOX concentration of 2 $\mu\text{g/mL}$. At predetermined intervals, the cells

Page 9 of 30

1 were washed with PBS and fixed with 4% (w/v) paraformaldehyde aqueous solution
2 for 10 min. The slides were then stained with Hoechst 33258 (5 mg/mL in PBS) at
3 37°C for 10 min. The fixed cell monolayer was finally observed by CLSM.

4 **2.7. Evaluation of cellular uptake by FCM**

5 The cellular uptake of the DOX-loaded nanoparticles was confirmed by
6 fluorescence microscopy (Epics XL). KB cells were incubated in six-well plates at a
7 density of 4.0×10^5 cells/well in 4 mL of folic acid deficient 1640 medium containing
8 10% FBS, and then cultured with the DOX-loaded nanoparticles with final DOX
9 concentration of 2 $\mu\text{g/mL}$. At predetermined intervals, the cells were washed with
10 PBS to remove the free nanoparticles that did not enter the cells prior to fluorescence
11 observation.

12 **2.8. In vitro cytotoxicity assay**

13 The vitro cytotoxicity of DOX-free nanoparticles or DOX-loaded nanoparticles
14 against KB cells and COS-7 cells was evaluated by the MTT assay. KB cells or
15 COS-7 cells were seeded into 96-well plate (Costar, IL, USA) at a density of 5.0×10^3
16 cells/well in 100 μL of folic acid deficient 1640 medium containing 10% FBS. The
17 cells were cultured for 1 day at 37°C in 5% CO_2 atmosphere. Afterwards, the cells
18 were incubated with DOX-free nanoparticles, DOX-loaded nanoparticles or free DOX.
19 After incubation, The 3-(4,5-dimethylthiazolyl-2)-2,5-diphenyltetrazo-lium bromide
20 (MTT) stock solution (5 mg/mL in PBS, 20 μL) was added to each well and incubated
21 for 4 h. The media were completely removed and 150 μL of DMSO was added to each
22 well to dissolve the formazan blue crystal. The absorbance of the solution was

Page 10 of 30

1 measured using a microplate reader at 570 nm. Cell viability was expressed as
2 follows:

3
$$\text{Cell viability (\%)} = A_{\text{sample}}/A_{\text{control}} \times 100\%.$$

4 Where A_{sample} and A_{control} are the absorbance values for the treated cells and the
5 untreated control cells, respectively. The A_{sample} and A_{control} values were obtained after
6 subtracting the absorbance of DMSO. Data are presented as average \pm SD (n = 4).

7 **2.9 Endocytosis inhibition**

8 KB cells were seeded on a 6-well plate at a density of 10^4 cells/well in 2 mL of
9 folic acid deficient 1640 medium containing 10% FBS. The cells were cultured for
10 24h at 37 °C in 5% CO₂ atmosphere. Then the cells were pretreated for 0.5h with
11 three different kind of endocytosis inhibitors separately (5 mM MBCD, 0.45 mM
12 sucrose, or 5mM cytochalasin D). After that, the NPs was added at a final DOX
13 concentration of 2 $\mu\text{g/mL}$. After incubation for 2 h, the cells were washed with PBS
14 and then were analysed by flow cytometry.

15 **2.10. Therapeutic studies in vivo**

16 Female athymic BALB/c-nu nude mice (4–6 weeks old, 18 ± 2 g) were housed
17 under specific pathogen-free conditions. Before treatment, all of the animals were kept
18 in quarantine for a week. To establish a tumor model, KB cells (1×10^7 per animal)
19 were subcutaneously injected into the flank region of mice. When tumors grew to a
20 volume of 50 mm^3 (about 10 days after inoculation), 24 mice were randomized into 4
21 groups and numbered. After that, 200 μL of DOX-loaded FLPNPs, DOX-loaded
22 LPNPs, free DOX (an equivalent dose of DOX 5 mg/kg) and PBS were injected

Page 11 of 30

1 through the tail vein, which was designated day 0.

2 Tumor volume size (V) was monitored every 2 d for up to 24 days. Tumor volume
3 was estimated by the following equation: $V = a \times b^2/2$, where a and b are the longest
4 and shortest diameters, respectively. The survival rates were also recorded.

5 **2.11. Distribution studies in vivo**

6 KB cells (1×10^7 per animal) were subcutaneously injected into the flank region
7 of mice to establish a tumor model. When the mean tumor volume reached
8 approximately 500 mm^3 , the tail intravenous administration of DOX-loaded
9 FLPNPs, DOX-loaded LPNPs free DOX or PBS was performed at a dose of 5 mg
10 DOX/kg. At the designated time, the treatment group ($n = 4$) were killed and then
11 tumor, liver, spleen, heart, lung, and kidney were collected. The DOX in tissue was
12 extracted according to a predetermined method in literature.^{29, 30} Briefly, The organs
13 were weighed and homogenized with an Ultra-Turrax Homogenizer (IKA T25, 12500
14 rpm) in KH_2PO_4 solution ($20 \times 10^{-3} \text{ M}$, pH 2.8). Then, the tissue homogenate (200 μL ,
15 10% (w/v)) was exposed to an acidic hydrolysis in 50 μL of HCl (5 M) at 60 °C for
16 1.5h, After that, 50 μL of 1 M NaOH was added. The DOX in the mixture was
17 extracted using chloroform and isopropanol (4:1, v/v). The organic layer was
18 collected by centrifugation(12 000g, 8 min) and evaporated to dryness under vacuum.
19 The residue was dissolved in 200 μL of mobile phase (acetonitrile/water, 55:45, v/v)
20 and followed by HPLC analysis. To generate the control group, free DOX was added
21 to the tissues from untreated mice. The following processing of control group was the
22 same to described above.

Page 12 of 30

1 2.12. Statistical analysis

2 Empirical data are expressed as mean \pm SEM (error bars) from at least 3
3 independent experiments. For all analyses, if $P < 0.05$, results were considered
4 significantly different, as described in each figure legend.

5

6 3 RESULTS AND DISCUSSION

7 3.1 Preparation, characterization and reduction-triggered disassembly of 8 FLPNPs

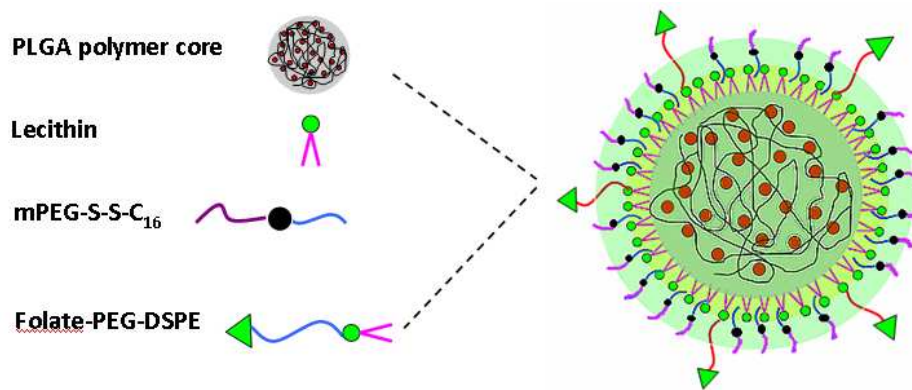
9 Although lipid-polymer hybrid nanoparticles have been widely investigated and
10 applied in drug delivery, stimuli-sensitive lipid-polymer hybrid nanoparticles have not
11 been developed. Based on the fact that PLGA- lecithin are unstable in PBS buffer and
12 become stable in PBS buffer after the introduction of a hydrophilic outer layer, we
13 expected that the introduction of sensitive lipid outer layer on the surface of PLGA-
14 lecithin surface will result in sensitive lipid-polymer hybrid nanoparticles. We here
15 introduced reduction-sensitive polymer mPEG-S-S-C₁₆ into PLGA- lecithin to
16 construct reduction lipid-polymer hybrid nanoparticles. After incubation of
17 mPEG-S-S-C₁₆ containing lipid-polymer hybrid nanoparticles under reductive
18 conditions, PEG segments are removed and the residual nanoparticles become
19 unstable again, and the aggregation occur to result in the fast release of encapsulated
20 drug in the hydrophobic parts of lipid-polymer hybrid nanoparticles.

21 In this work, folate-targeted LPNPs (FLPNPs) were prepared via modified
22 single-step assembly method. The FLPNPs were made up of three components (Fig.

Page 13 of 30

1 1): a hydrophobic PLGA core, a soybean phosphatidylcholine and a modified
2 hydrophilic polyethylene glycol (PEG) shell. The reduction-sensitive polymer
3 (mPEG-S-S-C₁₆) and the targeted ligand (DSPE-PEG_{2k}-Folate) were interspersed
4 throughout the lecithin monolayer.

5



6

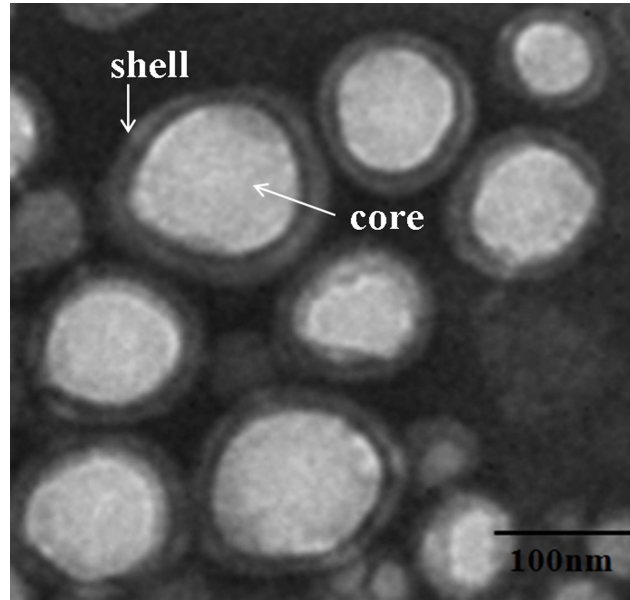
7 **Fig.1.** The schematic drawing of folate-targeted redox-sensitive lipid-shell and
8 polymer-core nanoparticles (FLPNPs).

9 As expected, a clear core-shell structure with smooth surface and spherical shape
10 could be observed from TEM (Fig. 2A). The hydrophilic lipid shell is fused about
11 8-15 nm on the hydrophobic PLGA core. The merit of this structure is that poorly
12 water-soluble drugs can be encapsulated highly efficiently into the hydrophobic
13 PLGA cavity. The nanoparticles can be well-dispersed in phosphate buffer solution
14 (PBS) with high stability, but they were unstable after removing the
15 reduction-sensitive PEG-shell. The TEM images show that the NPs were dispersed
16 with a well-defined spherical shape (Fig. 2). The size and size distribution of FLPNPs
17 were characterized by dynamic light scattering (DLS) and the results are listed in Fig.
18 3 and Table 1. The average size was generally in the same range (100-120 nm), which

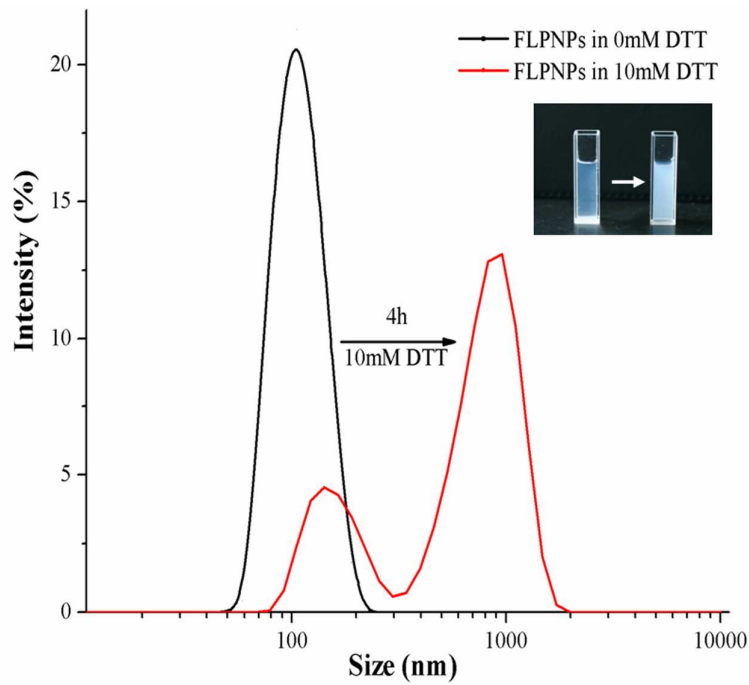
Page 14 of 30

1 is conducive to a satisfactory drug accumulation in tumor site through the enhanced
2 permeability and retention effect (EPR).³¹ The polydispersity of FLPNPs was 0.12,
3 which indicated a unimodal size distribution. The zeta potential of FLPNPs was -8.5
4 ± 2.4 mV.

5 In order to examine the reduction-triggered disassembly performance of FLPNPs,
6 the change of average size of FLPNPs and reduction-insensitive FLPNPs in response
7 to 20 μ M and 10 mM DTT in PBS (0.01 M, pH = 7.4) was monitored by DLS. As
8 shown in Fig. 3, at 10 mM DTT, fast aggregation of sensitive NPs was observed.
9 After 4 h, due to the cleavage of the disulfide linkages, the size distribution of
10 sensitive FLPNPs significantly increased,³² indicating the falling off of hydrophilic
11 PEG shells from the FLPNPs and the enhanced destabilization of hydrophobic inner
12 core. Notably, at 20 μ M DTT, corresponding to the peak GSH concentration in
13 extracellular fluids,³³ the size distribution of FLPNPs showed no evident change.
14 However, the reduction-insensitive FLPNPs were stable upon exposure to 20 μ M and
15 10 mM DTT in PBS.



1
2 **Fig. 2.** The TEM micrographs of FLPNPs.



3
4
5 **Fig. 3.** The size change of FLPNPs in response to 10 mM DTT in PBS after 4 h (0.01

6 M, pH = 7.4) determined by DLS.

7

Page 16 of 30

1 **Table 1**

2 Physicochemical characterization of FLPNPs and LPNPs. Data represent mean \pm SD,
 3 n = 3.

| Samples | Particles size (nm) | Polydispersity (PDI) | Zeta potential (mV) | Encapsulatio n efficiency EE (%) | Loading efficiency LE(%) |
|---------|------------------------|-------------------------|---------------------------|--|--------------------------------|
| FLPNPs | 118 \pm 3 | 0.12 \pm 0.01 | -8.5 \pm 2.4 | 82 \pm 2 | 6.1 \pm 0.5 |
| LPNPs | 109 \pm 3 | 0.13 \pm 0.01 | -3.2 \pm 1.3 | 79 \pm 2 | 5.9 \pm 0.5 |

4

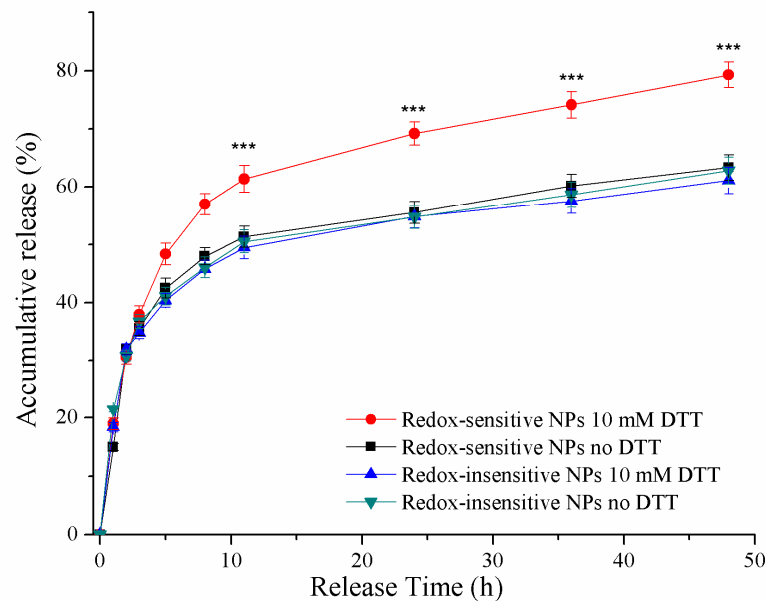
5 **3.2. DOX loading and in vitro reduction-triggered DOX release**

6 DOX as the most commonly used chemotherapeutic drug was loaded into
 7 FLPNPs as a model anticancer drug. The LE and EE of FLPNPs determined from
 8 three batches (Table 1) were 6.1 \pm 0.5% and 82.5 \pm 2% respectively.

9 Then the in vitro reduction responsive release behavior of the nanoparticles was
 10 investigated. The release of DOX from FLPNPs was studied using a dialysis tube
 11 (MWCO 8000). Dithiothreitol (DTT) was added to simulate a reductive environment
 12 such as cytosol and the cell nucleus. The cumulative releases are shown in Fig. 4. A
 13 burst release was observed at the early stage of the profiles, probably because DOX is
 14 more likely to diffuse from the PLGA core to the lipid monolayer.³⁴ Meanwhile, water
 15 molecules permeated into the hydrophilic parts of lipid monolayers, which led to the
 16 diffusion of drugs. Due to the cleavage of the disulfide linkages, obvious different
 17 release behaviors were observed in the FLPNPs with or without the reducing reagent
 18 (DTT) (Fig. 4). For FLPNPs, compared with 63% of drug release with the absence of

Page 17 of 30

1 DTT, about 79% of the payload was released after incubation for 48 h with the
2 presence of 10 mM DTT, implying that DOX was effectively released from the
3 FLPNPs in response to reductive environment of intracellular fluids in cancer cells.
4 This result confirmed the GSH-responsive degradation of mPEG-S-S-C₁₆, which
5 resulted in the dissociation of the nanoparticle structure. However, there
6 is no distinct change in the drug release of reduction-insensitive FLPNPs with or
7 without 10 mM DTT. Notably, 20 μ M DTT, corresponding to the peak GSH
8 concentration in extracellular fluids, will not result in significant change in the drug
9 release of FLPNPs (data not shown). These results suggested that the FLPNPs are
10 potential intracellular environment-sensitive drug nanocarriers.



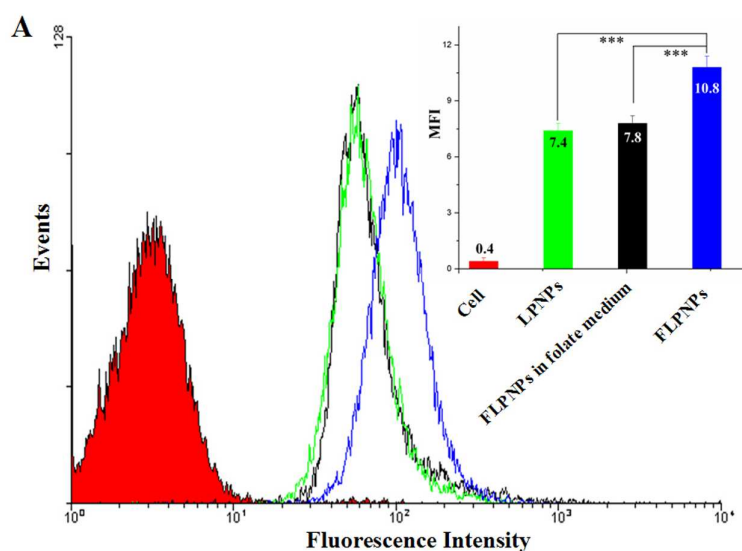
11

12 **Fig. 4.** Redox-triggered release of DOX from FLPNPs and Redox-insensitive FLPNPs
13 in PBS (0.01 M, pH 7.4) or with 10 mM DTT. Mean \pm SEM, ***, $p < 0.001$ versus
14 control.

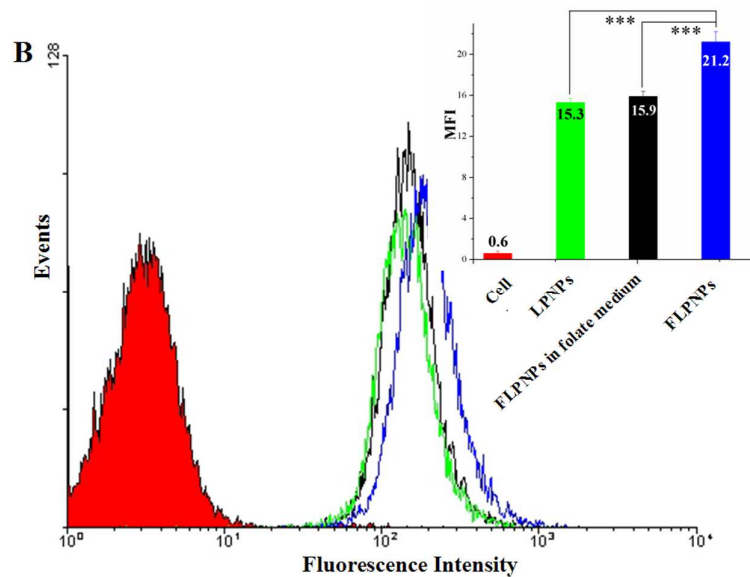
15 **3.3. In vitro cellular uptake**

Page 18 of 30

1 The targeted cellular uptake and intracellular reduction responsive drug release
2 profiles of DOX-loaded FLPNPs were examined with folate-overexpressing KB cells
3 and folate-deficient COS-7 cells using flow cytometry. The mean DOX fluorescence
4 was 21.2 or 10.8 after 4 or 10 h of incubation with FLPNPs in absence of folate,
5 which corresponded to 15.3 or 7.4 for LPNPs (Fig. 5). Irrespective of the incubation
6 time (4 or 10 h), the KB cells incubated with FLPNPs showed stronger DOX
7 fluorescence than those incubated with LPNPs. The results showed the selective
8 targeting ability of FLPNPs against KB cells. We also examined the effects of the
9 addition of folate into the medium. However, with the presence of folate in culture
10 medium, the cellular uptakes of DOX in FLPNPs were nearly the same as LPNPs.
11 As a result of competitive binding to FRs, the presence of folate prevented FLPNPs
12 from transporting into KB cells. These results fully proved that FLPNPs were
13 transported to cells by an FR-mediated endocytosis process.



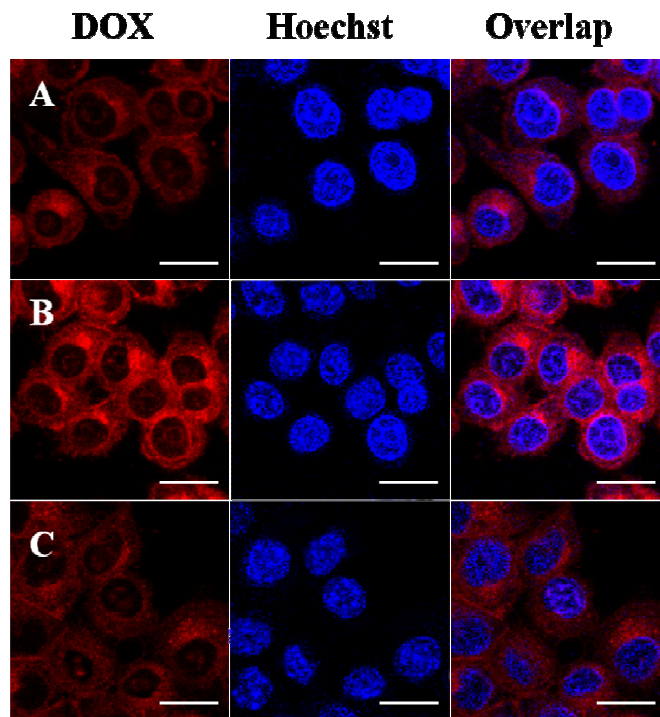
14



1

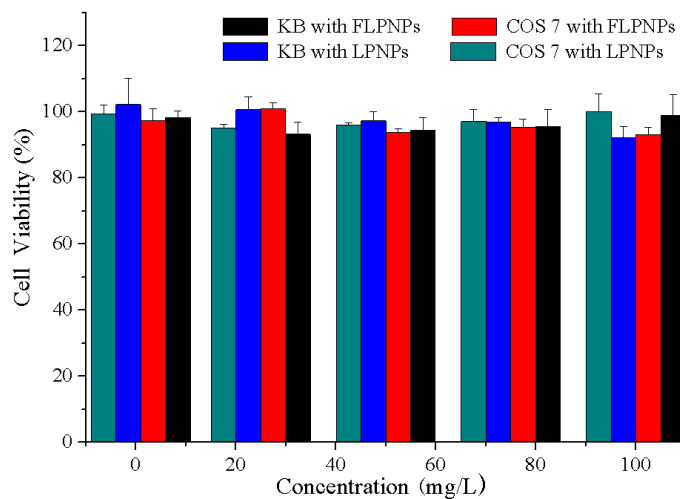
2 **Fig. 5.** Flow cytometry analyses of KB cells incubated with FLPNPs and LPNPs for 4
3 h (A) or 10 h (B), DOX dosage was 2 $\mu\text{g}/\text{mL}$. Mean \pm SEM, ***, $p < 0.001$ versus
4 control.

5 Cellular uptakes of FLPNPs and LPNPs by KB cells were further studied by
6 confocal microscopy. Fig. 6 clearly shows that FLPNPs produced stronger DOX
7 fluorescence than LPNPs after 10 h of incubation. In addition, it can be seen clearly
8 that FLPNPs were primarily located on the cell membrane, due to their
9 folate-targeting effect. Moreover, when KB cells were incubated in the folate medium,
10 the cellular uptake extent of FLPNPs was similar to that of LPNPs. The above results
11 are consistent with Fig. 5. Hence, it is reasonable to say that folate on the surface of
12 FLPNPs facilitated the entry of FLPNPs into cells.



1

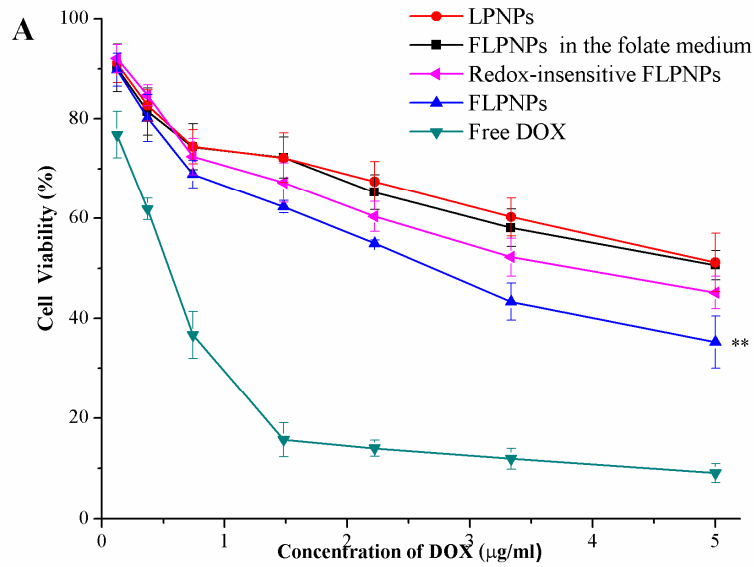
2 **Fig. 6.** Confocal laser scanning microscopy images of KB cells after treatment with
 3 LPNPs (A) , FLPNPs (B) and FLPNPs in the folate medium (C) for 10 h. Scale bar is
 4 20 μ m.



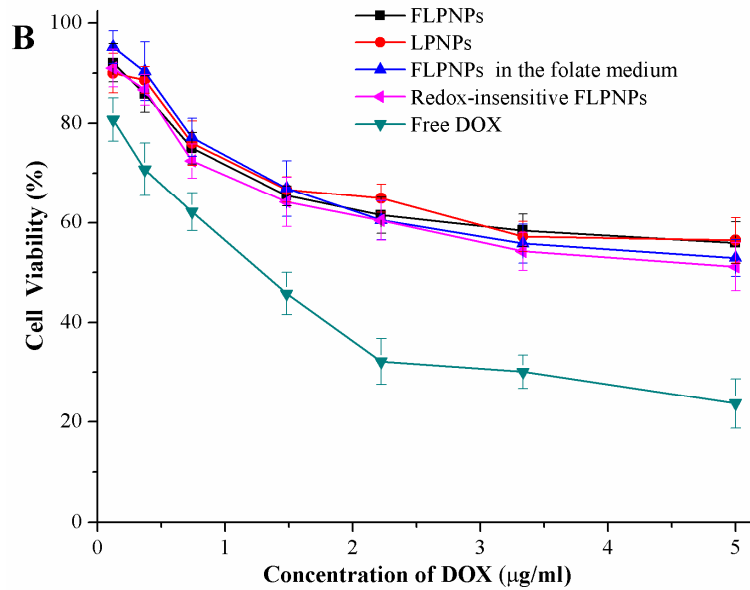
5

6 **Fig. 7.** MTT assay of FLPNPs and LPNPs in KB cells and COS-7 cells after
 7 incubation for 48 h (n = 4).

8 **3.4. In vitro cytotoxicity assay**



1



2

3 **Fig. 8.** Cytotoxicity of FLPNPs, LPNPs, Redox-insensitive FLPNPs, FLPNPs in the
 4 folate medium (0.2mM free folate was added to the nutrient medium) and free DOX
 5 against KB cells (A) and COS 7 cells (B) after incubation for 10 h ($n = 4$). Mean \pm
 6 SEM, **, $p < 0.01$ versus control.

7 KB cells or COS-7 cells were incubated with DOX-free FLPNPs or DOX-free
 8 LPNPs at different concentrations. MTT assays illustrated that this type of

Page 22 of 30

1 nanoparticles slightly affected the survival rate of KB cells and COS-7 cells in a
2 concentration-independent way (Fig. 7). The result proves the noncytotoxicity of the
3 two types of nanoparticles.

4 The cytotoxic effects of FLPNPs, LPNPs and free DOX against KB cells were
5 evaluated by MTT assay. All materials notably inhibited the growth of KB cells (Fig.
6 8A). The inhibitory effects on the cell viability were dose-dependent. The IC_{50} values
7 of FLPNPs, reduction-insensitive FLPNPs, LPNPs, and free DOX were about 2.7, 3.8,
8 5.2, and 0.5 $\mu\text{g/mL}$, respectively. Obviously, since small molecules can be more
9 easily transported into cells and nuclei via passive diffusion, free DOX was more
10 cytotoxic to KB cells than the nanoparticles.^{26, 34} However, at the same DOX
11 concentration, the cytotoxicity of FLPNPs was significantly higher than that of LPNPs,
12 which was consistent with the results observed by confocal laser scanning microscopy
13 (CLSM) and flow cytometry. Moreover, with the presence of 2 mM folate in the
14 medium, the cytotoxicity of FLPNPs was noticeably reduced and was nearly
15 equivalent to that of LPNPs. In addition, when FRs-negative COS-7 cells were
16 incubated with FLPNPs and LPNPs separately, no significant difference was found in
17 the cytotoxicity (Fig. 8B), which indicated that the cell uptake of FLPNPs was an
18 FRs-mediated endocytosis process.

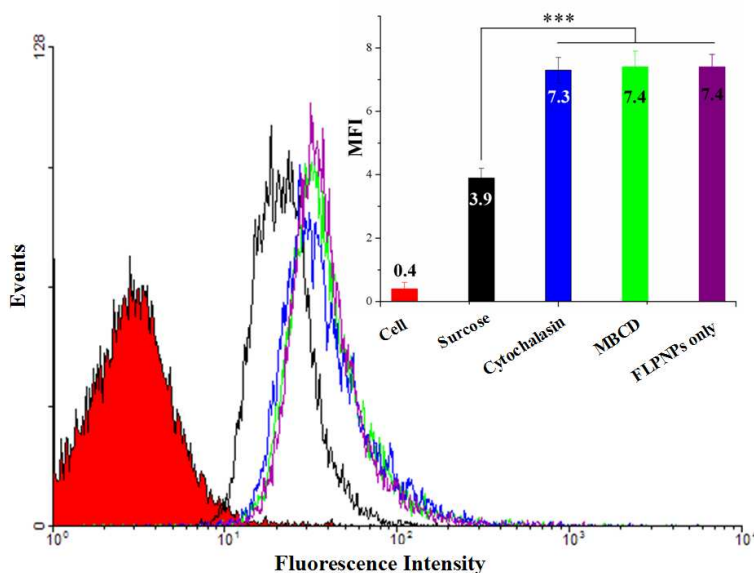
19 As an important control experiment, the cytotoxicity of reduction-insensitive
20 FLPNPs was also evaluated. As expected, the sensitive FLPNPs has obvious
21 advantages in average inhibiting rate of KB cells, as compared with the
22 reduction-insensitive FLPNPs. The IC_{50} values of FLPNPs, reduction-insensitive

Page 23 of 30

1 FLPNPs and LPNPs were about 2.7 and 3.8 $\mu\text{g}/\text{mL}$. The enhanced cytotoxicity of
2 FLPNPs revealed that the reduction-sensitive NPs are more efficient for intracellular
3 delivery of DOX as compared to insensitive control.

4 3.5. Endocytosis inhibition

5 Three types of endocytosis inhibitors were used to study the internalization
6 pathways of FLPNPs. MBCD was used as a caveolae-mediated endocytosis inhibitor,
7 hypertonic sucrose as a clathrin-mediated endocytosis inhibitor, and cytochalasin D as
8 a macropinocytosis inhibitor.³⁵ KB cells were incubated with FLPNPs in the presence
9 or absence of endocytosis inhibitors for 2 h. Fig. 9 shows that after treatment with
10 hypertonic sucrose, the mean DOX fluorescence intensity in KB cells significantly
11 decreased to 52%, while those of MBCD and cytochalasin D did not change.



12

13 **Fig. 9.** Effect of endocytosis inhibitors on the uptake of FLPNPs in KB cells using
14 flow cytometry analyses. DOX dosage was 2 $\mu\text{g}/\text{mL}$. Mean \pm SEM, ***, $p < 0.001$
15 versus control.

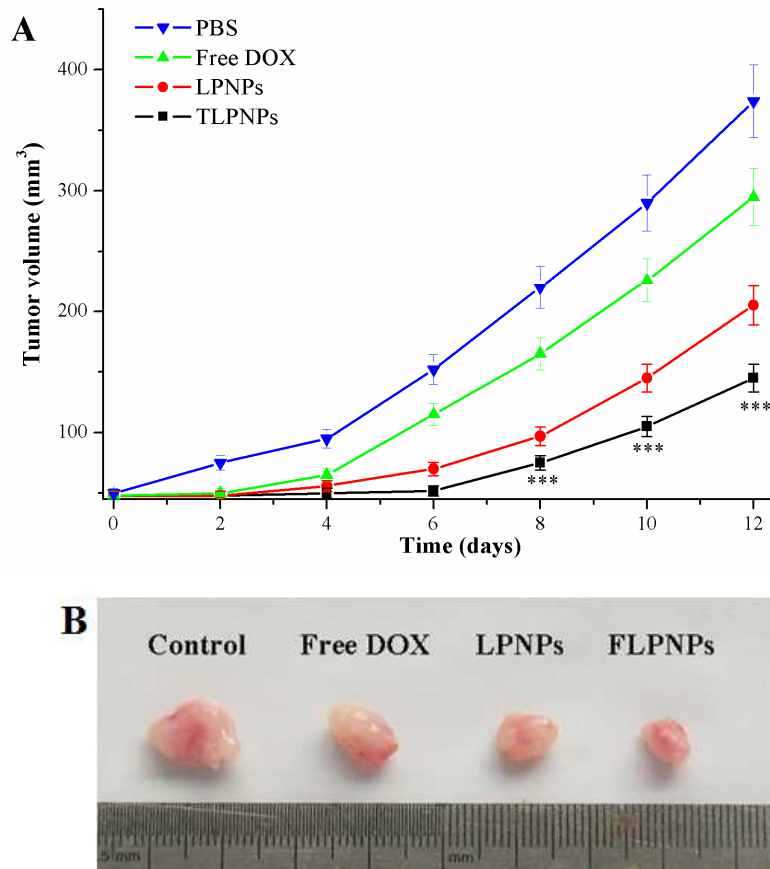
Page 24 of 30

1 Fig. 9 showed the presence of hypertonic sucrose obviously prevented the entry of
2 FLPNPs. The facts demonstrated that the pathway of FLPNPs into cells depended on
3 clathrin-mediated endocytosis. Clathrin-mediated endocytosis is the most highly
4 regulated and the fastest pathway of the internalization of integral membrane proteins.
5 The results were consistent with previous study.³⁶

6 **3.6. Therapeutic studies in vivo**

7 To demonstrate the targeted and antitumor efficacy efficacy of FLPNPs, we
8 developed KB cells xenografted on female athymic BALB/c-nu nude mice. When
9 tumors grew to a volume of 50 mm³ (about 10 days after inoculation), 24 mice were
10 randomized into 4 groups and numbered. After that, 200 μL of DOX-loaded FLPNPs,
11 DOX-loaded LPNPs, free DOX (an equivalent dose of DOX 5 mg/kg) and PBS were
12 injected through the tail vein, which was designated day 0. The growth of tumors was
13 observed for 12 days after separate treatments with FLPNPs, LPNPs and free DOX
14 (Fig. 10). Each treatment affected tumor growth compared with the control group
15 (treatment with PBS). As seen in Fig. 10A, the most effective therapeutics against KB
16 cells xenografted was the FLPNPs. At 12 days after injection, the average tumor
17 volume increased to about 205, 295, and 374 mm³ after treatment with LPNPs, free
18 DOX and PBS, respectively, but was only 145 mm³ after treatment with FLPNPs (Fig.
19 10A). The in vivo efficacy data showed that folate-targeted FLPNPs are more
20 effective than their non-targeted LPNPs in this murine model. This result is consistent
21 with our expectation. A combined effect of passive targeting and responsive release
22 would mainly explain the inhibition of tumor growth. Because of the EPR effect of

1 nanoparticles, FLPNPs and LPNPs showed more significant antitumor efficacy than
2 free DOX against KB cells xenografted. The in vivo animal experiments
3 demonstrated the significant antitumor efficacy of DOX-loaded FLPNPs.



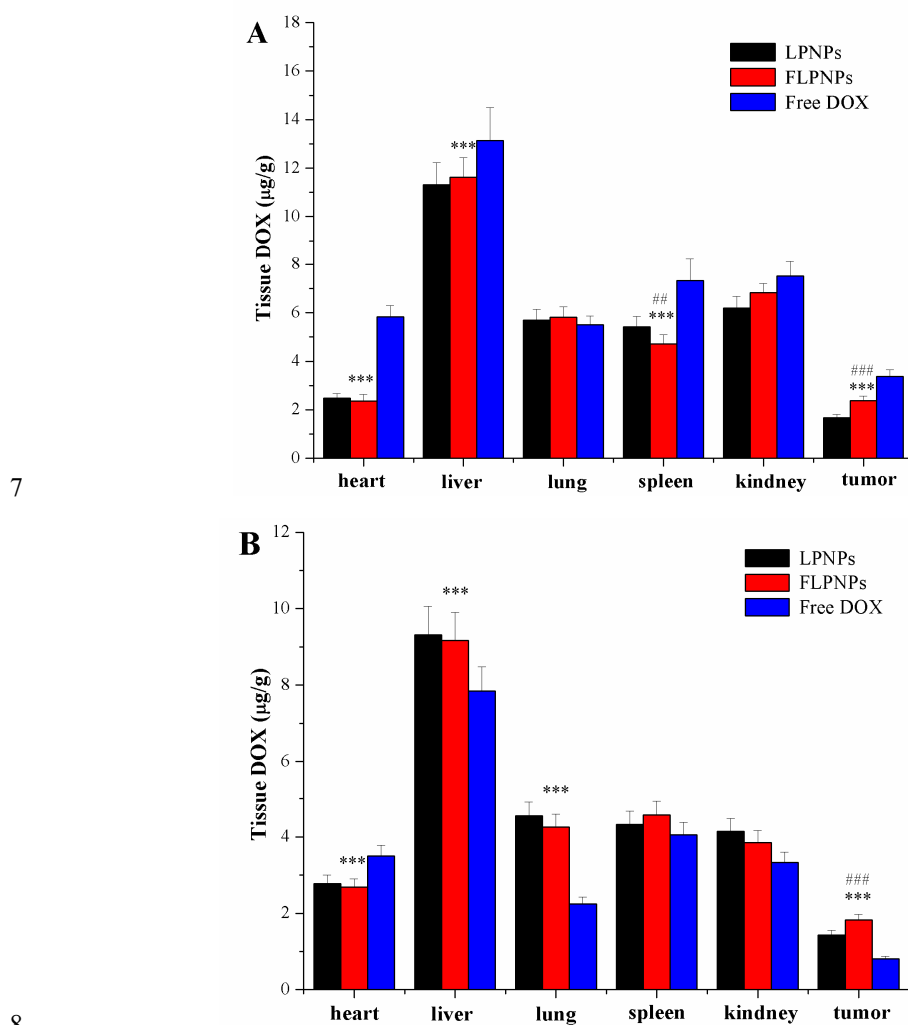
6 **Fig. 10.** (A) Antitumor effect of free DOX, FLPNPs and LPNPs on KB cell
7 xenografted. Mean \pm SEM, ***, $p < 0.001$ versus PBS group. (B) typical photographs
8 of excised tumors from the tested groups.

9 3.7 Biodistribution studies in vivo

10 In order to examine the accumulation at tumor site through passive targeting, the
11 concentrations of DOX in tumor, the spleen, liver, kidney, heart and lung were
12 measured after tail intravenous injection of DOX-loaded FLPNPs, DOX-loaded
13 LPNPs, and free DOX separately. For free DOX, the amount of DOX in the tumor

Page 26 of 30

1 was 3.38 $\mu\text{g/g}$ at 5 h, and it quickly decreased to 0.81 $\mu\text{g/g}$ at 12 h (Fig. 11). In contrast,
 2 after administration of DOX-loaded FLPNPs or DOX-loaded LPNPs, the amount of
 3 DOX in the tumor did not decrease but slightly increased with time. The amount of
 4 DOX in the tumor was 2.31 $\mu\text{g/g}$ at 12 h after administration of FLPNPs, and the level
 5 was much higher than free DOX (0.81 $\mu\text{g/g}$). This result suggested that this type of
 6 FLPNPs tend to accumulate at tumors site by the EPR effect of nanoparticles.



9 **Fig. 11.** Biodistribution profiles of DOX at 5 h (A) and 12 h (B) after free DOX,
 10 FLPNPs and LPNPs were injected via tail intravenous (n = 3). Mean \pm SEM, ***, p <
 11 0.001 versus free DOX group, ##, p < 0.01 and ###, p < 0.001 versus LPNPs group.

Page 27 of 30

1 In addition, there was a higher concentration of DOX in the tumors administered
2 with FLPNPs compared with LPNPs. FLPNPs exhibited a higher capability of DOX
3 accumulation at tumor site than LPNPs, suggesting that the transport of FLPNPs
4 through receptor-mediated endocytosis was more efficient than the transport of
5 LPNPs. This enhanced DOX accumulation profile in the tumor may be the main
6 reason explaining the higher antitumor efficacy of FLPNPs shown in Fig. 9. These
7 results fairly accorded with some previous experimental reports.^{29, 37}

8 In addition, the biodistribution profiles in other tissues were also measured (Fig.
9 11). The drug concentrations of both FLPNPs and LPNPs in the heart were lower than
10 that of free DOX, indicating that the side effects of DOX in the heart might be
11 reduced by this type of nanoparticles. The amount of DOX in the liver was
12 significantly higher than in any other tissue, which agreed with previous reports.³³

13

14 **4. Conclusions**

15 A novel type of folate-targeted redox-sensitive lipid-shell and polymer-core
16 nanoparticles (FLPNPs) was prepared for delivery of tumor-targeted drugs. The
17 FLPNPs had high monodispersity, high size stability and a clear core-shell structure.
18 The FLPNPs remarkably enhanced cell uptake and produced higher cytotoxicity
19 against folate-overexpressing KB cells, which were mainly attributed to a
20 folate-receptor-mediated endocytosis process. Furthermore, in vivo animal
21 experiments confirmed the noticeable antitumor efficacy and higher tumor
22 accumulation capability of FLPNPs.

Page 28 of 30

1

2 **AUTHOR INFORMATION**

3 **Corresponding Author**

4 Tel:+86 02768755317 fax: +86 02768755317

5 * E-mail Address: sw Huang@whu.edu.cn

6

7 **ACKNOWLEDGMENTS**

8 This work was financially supported by National Natural Science Foundation of
9 China (51473127, 51273150) and National Basic Research Program of China
10 (2011CB606202).

11

12 **References**

- 13 1. R. H. Fang, S. Aryal, C. J. Hu and L. Zhang, *Langmuir*, 2010, **26**, 16958-16962.
14 2. N. Chaubey, A. K. Sahoo, A. Chattopadhyay and S. S. Ghosh, *Biomater. Sci.*,
15 2014, **2**, 1080-1089.
16 3. Z. Chu, S. Zhang, C. Yin, G. Lin and Q. Li, *Biomater. Sci.*, 2014, **2**, 827-832.
17 4. P. M. Valencia, P. A. Basto, L. Zhang, M. Rhee, R. Langer, O. C. Farokhzad and
18 R. Karnik, *ACS nano*, 2010, **4**, 1671-1679.
19 5. L. Zhang, J. M. Chan, F. X. Gu, J. W. Rhee, A. Z. Wang, A. F. Radovic-Moreno, F.
20 Alexis, R. Langer and O. C. Farokhzad, *Acs Nano*, 2008, **2**, 1696-1702.
21 6. J. M. Chan, L. Zhang, K. P. Yuet, G. Liao, J. W. Rhee, R. Langer and O. C.
22 Farokhzad, *Biomaterials*, 2009, **30**, 1627-1634.
23 7. L. Zhang, J. M. Chan, F. X. Gu, J. W. Rhee, A. Z. Wang, A. F. Radovic-Moreno, F.

Page 29 of 30

- 1 Alexis, R. Langer and O. C. Farokhzad, *ACS Nano*, 2008, **2**, 1696-1702.
- 2 8. J. Pan and S. S. Feng, *Biomaterials*, 2009, **30**, 1176-1183.
- 3 9. A. R. Hilgenbrink and P. S. Low, *J. Pharm. Sci.*, 2005, **94**, 2135-2146.
- 4 10. V. Dixit, J. Van den Bossche, D. M. Sherman, D. H. Thompson and R. P. Andres,
5 *Bioconjugate Chem.*, 2006, **17**, 603-609.
- 6 11. D. Li, Y. T. Zhang, S. Jin, J. Guo, H. F. Gao and C. C. Wang, *J. Mater. Chem. B*,
7 2014, **2**, 5187-5194.
- 8 12. X. Yang, J. J. Grailer, S. Pilla, D. A. Steeber and S. Gong, *Bioconjugate Chem.*,
9 2010, **21**, 496-504.
- 10 13. X. Chen, X. Cheng, A. H. Soeriyadi, S. M. Sagnella, X. Lu, J. A. Scott, S. B.
11 Lowe, M. Kavallaris and J. J. Gooding, *Biomater. Sci.*, 2014, **2**, 121-130.
- 12 14. A. Beaussart, T. C. Ngo, S. Derclaye, R. Kalinova, R. Mincheva, P. Dubois, P.
13 Leclere and Y. F. Dufrene, *Nanoscale*, 2014, **6**, 565-571.
- 14 15. S. Febvay, D. M. Marini, A. M. Belcher and D. E. Clapham, *Nano Lett.*, 2010, **10**,
15 2211-2219.
- 16 16. X. L. Wu, J. H. Kim, H. Koo, S. M. Bae, H. Shin, M. S. Kim, B.-H. Lee, R.-W.
17 Park, I. S. Kim and K. Choi, *Bioconjugate Chem.*, 2010, **21**, 208-213.
- 18 17. M. C. Palanca-Wessels, A. J. Convertine, R. Cutler-Strom, G. C. Booth, F. Lee, G.
19 Y. Berguig, P. S. Stayton and O. W. Press, *Molecular Therapy*, 2011, **19**,
20 1529-1537.
- 21 18. P. C. Du, H. Y. Yang, J. Zeng and P. Liu, *J. Mater. Chem. B*, 2013, **1**, 5298-5308.
- 22 19. X. L. He, M. M. Ding, J. H. Li, H. Tan, Q. Fu and L. Li, *Rsc Advances*, 2014, **4**,
23 24736-24746.
- 24 20. F. Meng, W. E. Hennink and Z. Zhong, *Biomaterials*, 2009, **30**, 2180-2198.
- 25 21. Y. Z. You, C. Y. Hong and C. Y. Pan, *Macromolecules*, 2009, **42**, 573-575.
- 26 22. R. Cheng, F. Feng, F. Meng, C. Deng, J. Feijen and Z. Zhong, *J. Controlled*
27 *Release*, 2011, **152**, 2-12.
- 28 23. L. Brulisauer, M. A. Gauthier and J. C. Leroux, *J. Controlled Release*, 2014, **195**,
29 147-154.
- 30 24. S. Raina and D. Missiakas, *Annual Review of Microbiology*, 1997, **51**, 179-202.

Page 30 of 30

- 1 25. W. Chen, P. Zhong, F. Meng, R. Cheng, C. Deng, J. Feijen and Z. Zhong, *J.*
2 *Controlled Release*, 2013, **169**, 171-179.
- 3 26. C. Cui, Y. N. Xue, M. Wu, Y. Zhang, P. Yu, L. Liu, R. X. Zhuo and S. W. Huang,
4 *Biomaterials*, 2013, **34**, 3858-3869.
- 5 27. P. Zhao, H. Wang, M. Yu, Z. Liao, X. Wang, F. Zhang, W. Ji, B. Wu, J. Han, H.
6 Zhang, H. Wang, J. Chang and R. Niu, *Eur. J. Pharm. and Biopharm.*, 2012, **81**,
7 248-256.
- 8 28. O. Taratula, A. Kuzmov, M. Shah, O. B. Garbuzenko and T. Minko, *J. Controlled*
9 *Release*, 2013, **171**, 349-357.
- 10 29. H. S. Yoo and T. G. Park, *J. Controlled Release*, 2004, **96**, 273-283.
- 11 30. C. Y. Sun, S. Dou, J. Z. Du, X. Z. Yang, Y. P. Li and J. Wang, *Advanced*
12 *healthcare materials*, 2013, **3**, 261-272.
- 13 31. Z. Gao, A. N. Lukyanov, A. Singhal and V. P. Torchilin, *Nano Letters*, 2002, **2**,
14 979-982.
- 15 32. J. Li, M. Huo, J. Wang, J. Zhou, J. M. Mohammad, Y. Zhang, Q. Zhu, A. Y.
16 Waddad and Q. Zhang, *Biomaterials*, 2012, **33**, 2310-2320.
- 17 33. G. K. Balendiran, R. Dabur and D. Fraser, *Cell biochemistry and function*, 2004,
18 **22**, 343-352.
- 19 34. Y. Liu, K. Li, J. Pan, B. Liu and S. S. Feng, *Biomaterials*, 2010, **31**, 330-338.
- 20 35. O. P. Perumal, R. Inapagolla, S. Kannan and R. M. Kannan, *Biomaterials*, 2008,
21 **29**, 3469-3476.
- 22 36. J. M. Oh, S. J. Choi, S. T. Kim and J. H. Choy, *Bioconjugate Chem.*, 2006, **17**,
23 1411-1417.
- 24 37. X. Yang, J. J. Grailer, I. J. Rowland, A. Javadi, S. A. Hurley, D. A. Steeber and S.
25 Gong, *Biomaterials*, 2010, **31**, 9065-9073.
- 26